Sensors and Materials, Vol. 9, No. 6 (1997) 363–378
MYU Tokyo

S & M 0298

Microchannels and Microcells for Gaseous Microsamples

Vassili Karanassios* and Jonathan T. Sharples

Guelph-Waterloo Center for Graduate Work in Chemistry, University of Waterloo, Department of Chemistry, Waterloo, Ontario, Canada N2L 3G1

(Received May 30, 1996; accepted October 14, 1996)

Key words: microchannel, <100> Si, UV transparent microcell, amorphous quartz, micromachining, microsamples, mercury-vapor, atomic fluorescence, miniaturization

Demand for chemical analysis systems with microsample handling capabilities needs little justification considering, for example, environmental monitoring where applications exist in abundance. When attempting to develop such systems, microsamples can be transported from an inlet, to a detector or a measurement "cell" and then to an outlet using an enclosed microchannel. Fabrication of such a channel using <100> Si wafers and 20% KOH is described. Coupling ultraviolet (UV) light to the enclosed microchannel has the potential to convert it into a cell for *in situ* measurement of chemical species traversing the channel. Fabrication of such a cell in quartz is presented. The enclosed cell was tested with microliter (μl) volumes of air-saturated-in-mercury (Hg)-vapor and non-dispersive atomic fluorescence spectrometry and the results were compared with those obtained using a commercially available milliliter (ml) volume cell. Significant improvements in detection limits were obtained by making the volume of the measurement cell comparable to that of the sample and were attributed to favorable effects of scaling laws.

1. Introduction

Transport of analytical samples from an inlet to a detector or a measurement "cell" and then to an outlet is mandatory for most chemical analysis systems regardless of their size. For systems with microsample analytical capabilities it is desirable, or even essential, for the volume of the transport channel and of the measurement cell to be comparable to that of the sample to be measured (or analyzed). A number of scientific and technological

* Author to whom correspondence should be addressed.

challenges arise when considering the size of such channels and cells. A key challenge is the choice of fabrication materials and technology. A convenient starting point is to borrow those used in the microelectronics industry.

The main objective of this work was to examine the possibility of using such technology to fabricate microliter (μl) volume channels in Si and UV-transparent measurement microcells in amorphous quartz.

2. Fabrication of a Microchannel

2.1 *Rationale*

The demand for and potential of chemical measurement systems with microanalytical capabilities are undisputed. For example numerous applications in environmental monitoring exist. In these types of systems, microsamples may be transported using enclosed microchannels. Fabrication of such a channel using single-crystal Si wafers is described below.

2.2 *Design of microchannel*

A schematic of the desired 12.5 μl volume enclosed microchannel is shown in Fig. 1 and an abbreviated fabrication sequence is shown in Fig. 2. The main channel (Figs. 1(d) and 1(e)) was 25 mm long, 2.5 mm wide and 200 μm deep. The channel was extended as long as possible to take advantage of the working area of the 3" wafer. To help characterize the etched walls of the channel, two secondary channels were added perpendicular to the main channel. It was anticipated that a thin wall would be formed (Figs. 1(d) and 1(e)) after etching between the main channel and the secondary channels.

2.3 *Choice of substrate*

Single crystal Si, as opposed to amorphous-Si or glass, was chosen due to its inertness to (relatively) harsh chemical environments, its desirable mechanical properties and chemical etching characteristics, as well as its compatibility with microelectronics. For example, readout electronics and a detector may be integrated on the same wafer as the microchannel or on the cover plate. The starting material was an n-doped (phosphorous), 3-inch, <100> silicon wafer with 356 – 406 μm nominal thickness and 1 – 2 Ω/cm resistivity.

2.4 *Pre-processing*

The wafer was cleaned to remove possible contaminants and a thin film (0.8 μm) of SiO_2 was thermally grown on it. The thin film passivates the surfaces of the wafer since most etching reagents have very low etch rates for silicon dioxide. Subsequent processing steps are schematically shown in Fig. 2 and are briefly described below.

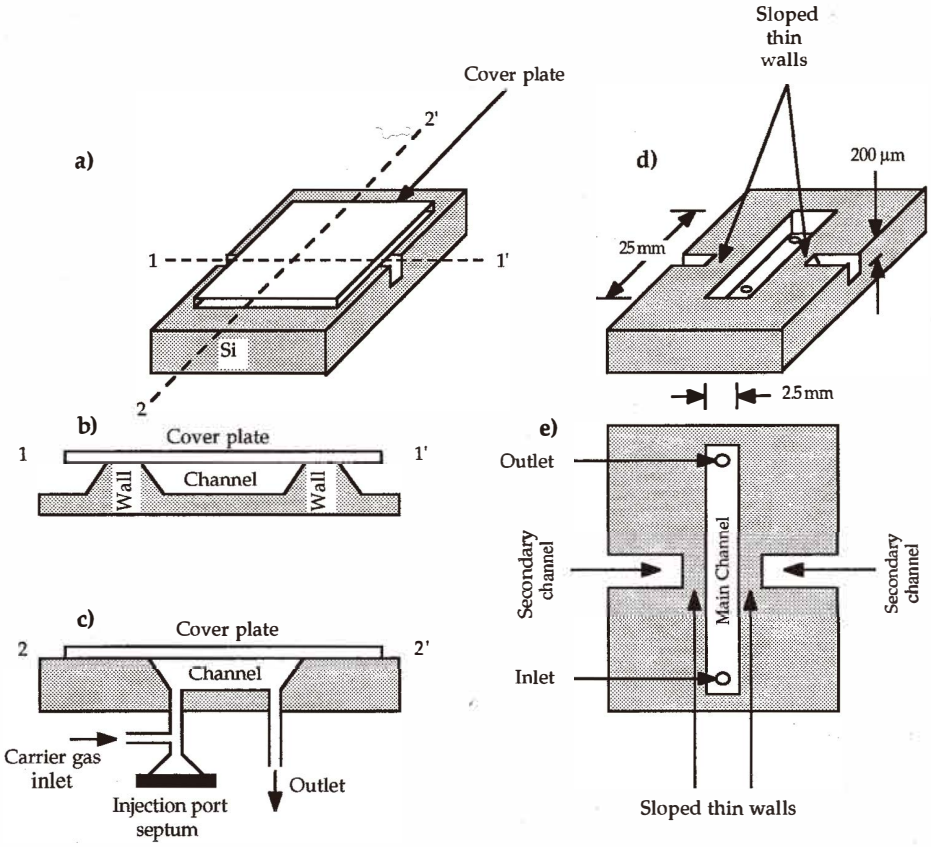

Fig. 1. Illustration (not to scale) of the enclosed microstructure in Si. (a) 3-d view of the enclosed microstructure (with the cover plate installed); (b) cross section across the 1, 1' axis shown in (a); (c) cross section across the 2, 2' axis shown in (a); (d) 3-d view of microchannel (with the cover plate removed) and (e) top view of microchannel shown in (d).

2.5 *Mask*

The channels and some additional test-patterns were designed using a commercially available drafting package (MacDraw Pro) on an Apple Macintosh computer. The design (Fig. 3) was produced on a 10:1 scale and was printed on an 11 by 11 inch mylar sheet using a high resolution (2400 dot-per-inch) printer. The design on the mylar was photo-reduced 10 times and was then transferred onto a glass plate "mask". With a one-step photo-reduction, the smallest feature on the mask was 30 μm.

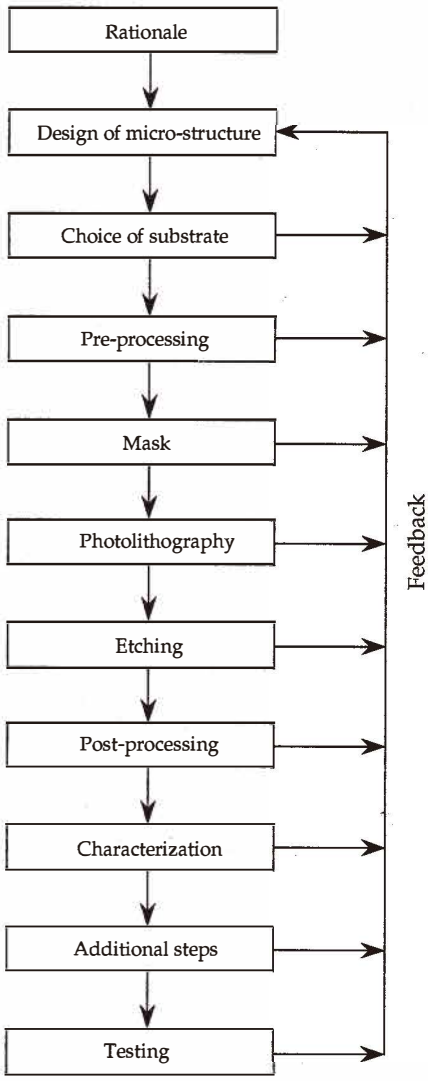

Fig. 2. Processing steps required for fabrication of the microstructures relevant to this work (see text for details). In this case and in contrast to conventional practice, the design of microstructure dictated the choice of substrate.

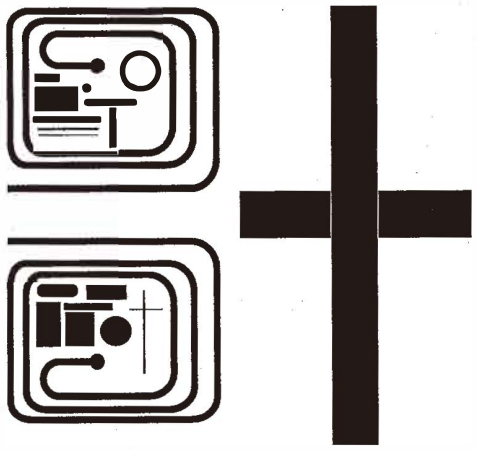

Fig. 3. Mask used for fabrication of the Si microchannel. Also shown are additional test patterns that were included to further characterize etching.

2.6 *Photolithography*

A light sensitive polymeric photoresist was spin coated on the top surface of the wafer to a thickness of about 1.2 μm. The wafer was placed on a mask aligner (Karl Süss, Model MJB3 UV400) and the mask was brought into contact with the top surface of the photoresist.

The black areas of the mask (Fig. 4(a)) prevent UV-light from the source of radiation from impinging on the photoresist, whereas the transparent ones permit light to pass through, thus solubilizing the exposed regions. After exposure to UV-light, the wafer was immersed in a developer solution and the solubilized areas of the photoresist were dissolved, leaving the underlying SiO_2 intact (Fig. 4(b)). Subsequently, the exposed SiO_2 layer (Fig. 4(b)) was etched-away (Fig. 4(c)) and the photoresist was stripped (Fig. 4(d)). Mask, pre-processing and lithography were performed in a class 1000 clean room in the Microelectronics Research Laboratory of this university.

2.7 *Wet chemical etching and post-processing*

The patterned wafers (Fig. 4(d)) were etched using a 20% KOH solution at 80°C for 200 min. The wafer was then removed from the etch-bath and thoroughly rinsed with 10 MΩ water. The SiO_2 masking layer (Fig. 4(e)) was removed, thus producing the desired etched shapes (Figs. 4(f) and 5).

2.8 *Characterization*

The etch depth was measured using a mechanical stylus profilometer (Sloan Dektak surface profiling system with fast leveling module) and was approximately 200 μm on

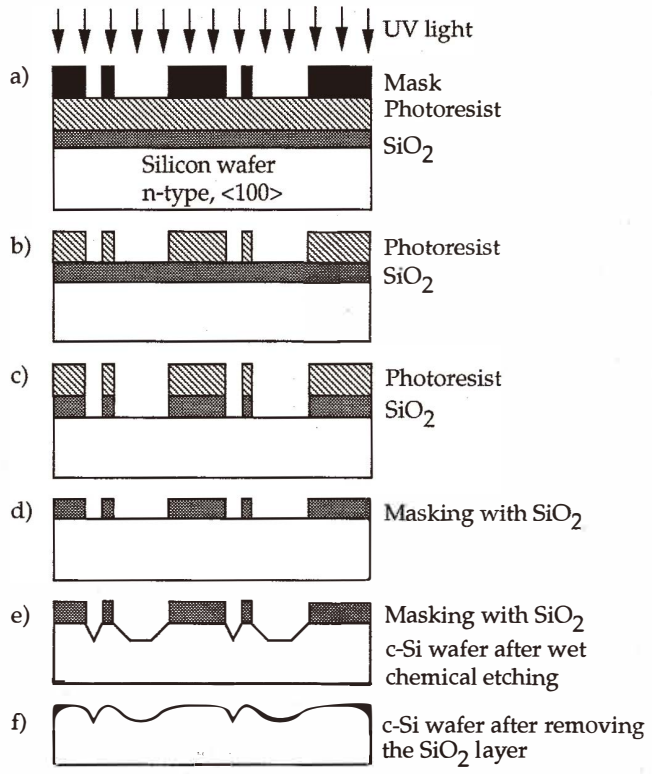

Fig. 4. Fabrication sequence of the Si microchannel (see text for details).

average. At this etch-depth, the width of the thin walls between the central and the perpendicular channels (Figs. 4(d), 4(e) and 5) varied from 30 μm at the top to 310 μm at the bottom of the channel.

The surface quality of the etched channels was characterized using a mechanical stylus profilometer, video microscopy and scanning electron microscopy (SEM). The integrity of the surface of the SiO_2 layer (Figs. 4(d) and 4(e)) and of the walls near a corner of the central channel were examined using SEM, and an etched corner of a microchannel is shown in Fig. 6. In some instances, under-etching of the SiO_2 layer was observed, the extent of which depended on the etchant composition and experimental conditions.

While mostly smooth surfaces were observed, depending on the etching conditions, pyramidal protrusions and (some) debris were also observed (Fig. 6). Although the debris may be removed by thorough rinsing, thus reducing the possibility of contamination of chemical species traversing the channel, pyramidal protrusions affect flow patterns and are more difficult to eliminate. One way of improving surface finish, increasing etch rate and

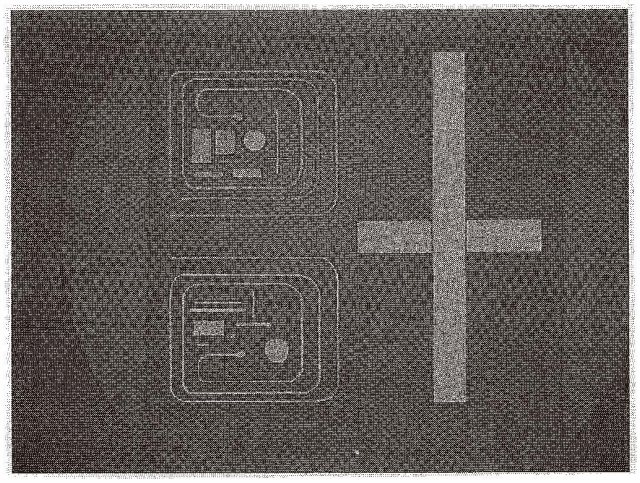

Fig. 5. Video-print showing the etched microchannel and the additional test structures on the Si wafer.

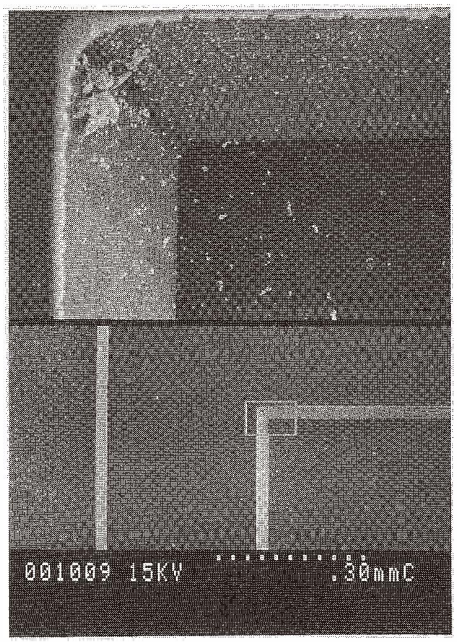

Fig. 6. SEM showing a corner and part of a microchannel etched in Si.

reducing debris and pyramidal protrusions is the use of ultrasonic agitation during etching.[1]

2.9 *Additional steps required for development of an enclosed microchannel*

The wafer was diced to size at the Microtechnology Research Laboratory. Two holes were drilled at either end of the bottom of each microchannel (Figs. 1(c), 1(d) and 1(e)) and two thin-wall stainless steel tubes were affixed to the cell. A septum was secured at one end of the inlet tube and a sliced wafer (that acted as a cover plate) was clamped to the microcell, thus producing an enclosed microchannel of the type shown in Fig. 1(a).

2.10 *Potential future applications*

By using a commercially available microsyringe and by injecting μl volumes of gases through the septum, the enclosed microchannel may be used as a low dead-volume sample introduction system, for example, for a thermal conductivity detector (TCD).[2] Integration of readout electronics and use of software, such as partial least squares[3] or neural networks,[4] to (partially) compensate for the lack of selectivity of the TCD detector, may result in an analytical measurement system that may be used in gas identification applications (*e.g.*, a gas-leakage monitor). Alternatively, sensing approaches that provide selectivity higher than a TCD may be used and an example is described below.

3. Fabrication of a UV-Transparent Microcell

3.1 *Rationale*

Since many chemical species have unique spectroscopic signatures, in particular, in the UV-visible regions of the electromagnetic spectrum, significant gains in selectivity may be obtained using spectroscopy. Coupling UV-visible light to the enclosed microchannel would allow *in situ* measurement of chemical species as they traverse a channel, thus forming a measurement microcell. Since single crystal Si is not transparent to UV-visible radiation, supplying light to the microchannel necessitates the use of a fiber-optic cable. This, however, complicates fabrication. Furthermore, UV-transmissive cables are not readily available, they have relatively poor transmission characteristics and may solarize upon prolonged irradiation by intense UV radiation. Is it possible to use a UV-transparent material for the development of a microcell that may be used for *in situ* spectroscopic measurement of gaseous analytes in μl volumes of air? This question was addressed as briefly described below.

3.2 *Design of the measurement microcell*

A three-dimensional view of the desired 37-μl UV-transparent measurement microcell is shown in Fig. 7. The cell consists of a channel and a cover plate. The main channel (Figs. 7(e) and 7(f)) is 365 μm deep, 20 mm long and 5 mm wide. Similar to the Si channel, a secondary channel was placed next to the main channel but unlike the Si channel, the secondary channel runs parallel to the main channel (Figs. 7(a), 7(e) and 7(f)). Furthermore, to ease installation of the gas inlet and outlet tubes (Fig. 7(d)), and to match the form

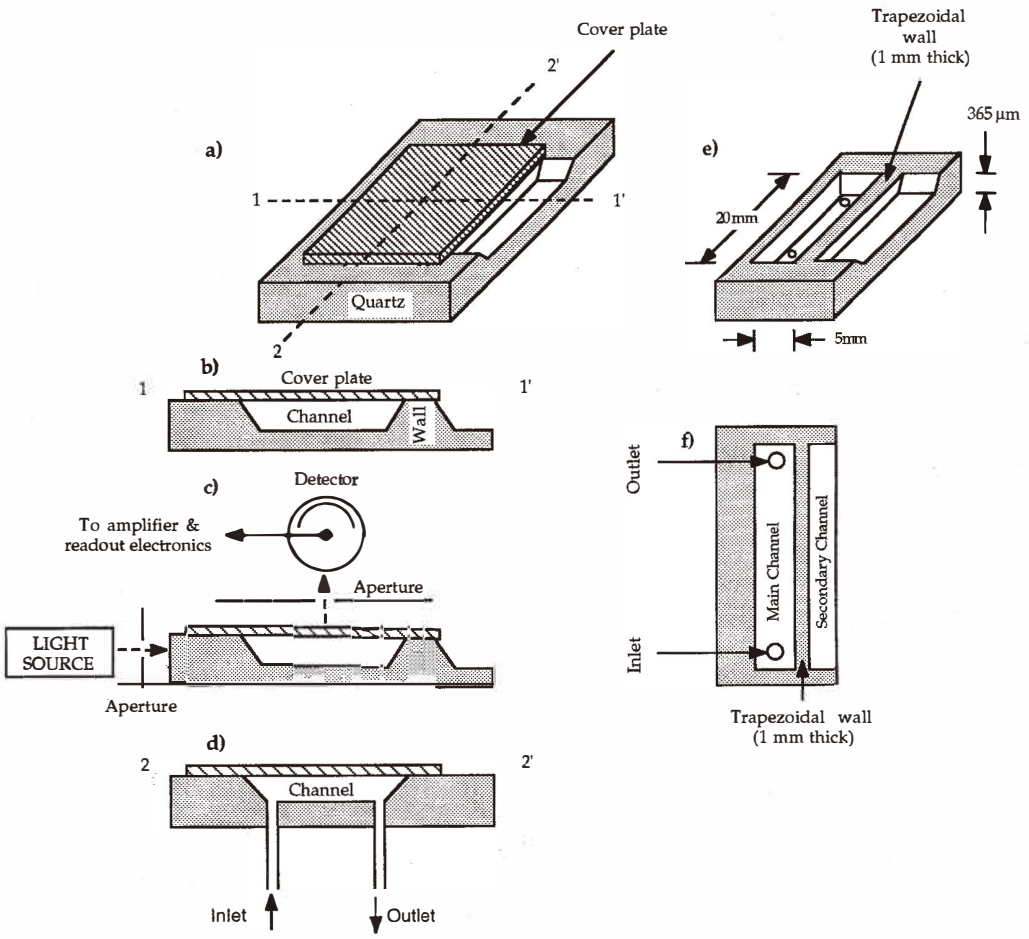

Fig. 7. Illustration (not to scale) of the enclosed, UV-transparent microcell. (a) 3-d view of enclosed microstructure (with the cover plate installed); (b) cross section across the 1, 1' axis shown in (a); (c) set up for fluorescence measurements; (d) cross section across the 2, 2' axis shown in (a); (e) 3-d view of microchannel (with the cover plate removed) and (f) top view of microchannel shown in (d).

factor of the photomultiplier tube (PMT) detector that was to be used for testing purposes, each channel was 5 mm wide. Also, the walls were extended to 1 mm, since a minimum separation between the channels was not necessary due to the high transmission of quartz at the wavelength of interest. The fabrication sequence (Fig. 2) is described in the following sections.

3.3 *Choice of substrate*

Amorphous quartz was chosen due its chemical inertness toward most analytes and its desirable optical properties. Fabrication of a UV-transparent microchannel will be used as an example of micromachining of quartz. The starting material was a 3-inch-diameter, optically flat quartz wafer with a nominal thickness of 1.6 mm.

3.4 *Pre-processing*

A thin film (800 Å) of Cr followed by a thin film (1 nm) of Au were sputter-deposited on the wafer, as is typically done for glass[5,6,7,8] micromachining and for wet chemical etching of AT-cut single-crystal quartz.[9]

3.5 *Mask*

The mask (Fig. 8) was prepared as described previously for Si. However, processing of the quartz wafer prior to transferring the design differed in several respects due to the use of different etchants. The process is illustrated in Fig. 9.

3.6 *Photolithography*

A "thick" layer of photoresist (1.8 microns rather than the typical 1.2 microns) was spun on the wafer, and the pattern was transferred onto the wafer.

3.7 *Wet chemical etching and post-processing*

After exposure to UV radiation and development of the photoresist, a mixture of KI and I_2 was used to remove the Au overlying the areas to be etched. Similarly, a $K_3Fe(CN)_6$

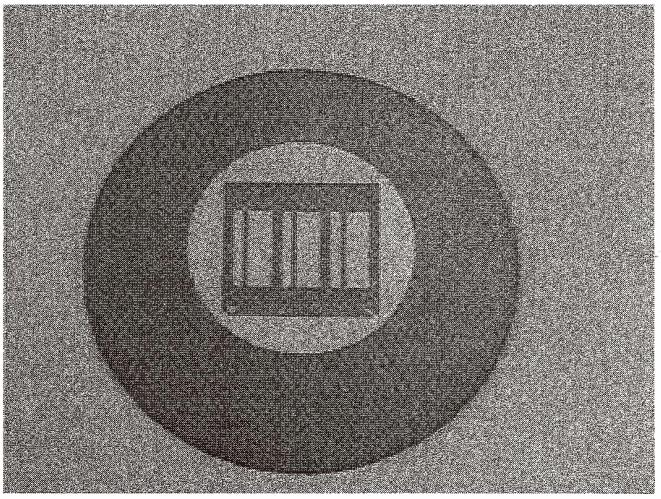

Fig. 8. Video-print of the mask used to pattern the quartz wafer.

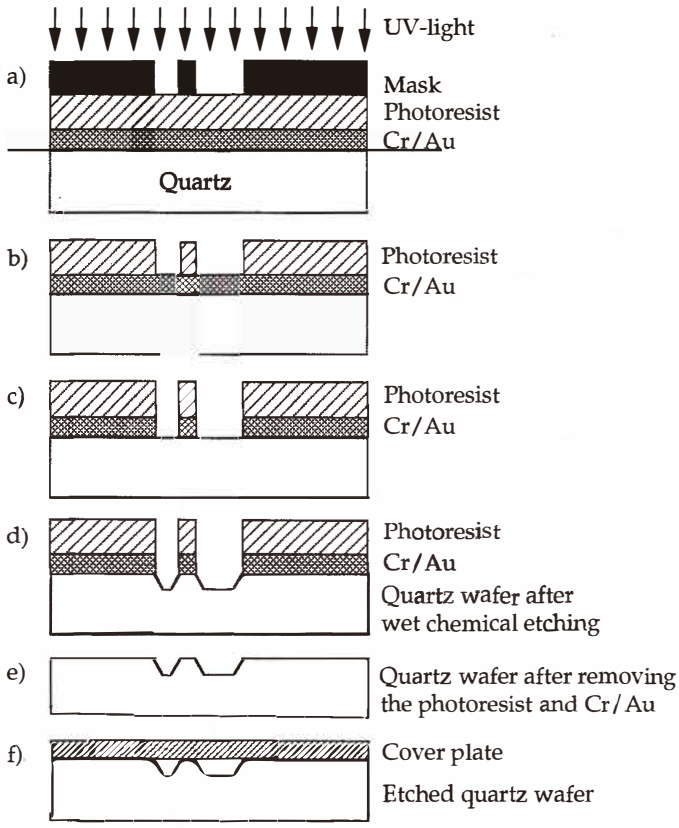

Fig. 9. Fabrication sequence of a quartz microcell (see text for details).

(potasium hexacyanoferrate (III) or potasium ferricyanide) and NaOH mixture was used to remove Cr. These etchants do not degrade the photoresist which was left on the wafer during etching to protect against HF-based etchants creating pinholes in the Au layer. Having exposed those areas intended to be etched, paraffin wax was applied to the backside of the wafer to protect it during etching.

Four etchant systems were evaluated with respect to etch rate and the quality of the etched surfaces. These were: concentrated HF (48%), dilute HF (1:2, 1:4 and 1:6 HF:H_2O), 7.2 M NH_4HF_2 (ammonium hydrogen fluoride), and 3.6 M NH_4HF_2 + 4.5 M H_2SO_4. Etch rate experiments were carried out using etchant solutions that were not stirred at room temperature for either 240 min (HF systems) or 180 min (NH_4HF_2 systems). The etch rate for the concentrated HF solution was approximately 1.5 μm/min and for the diluted HF solutions was 0.23, 0.20 and 0.11 μm/min. Surface quality was essentially the same

regardless of HF concentration. A similar quality was observed for the wafer that was etched with 3.6 M NH_4HF_2 + 4.5 M H_2SO_4, however, the etch rate was only 0.26 μm/min. The etch rate for 7.2 M NH_4HF_2 was 0.40 μm/min but the surface quality was poor, for example, the etched surfaces were severely frosted (essentially, they were non-transparent). As a consequence, concentrated HF (48%) was used. As before, the patterned wafer was suspended in an unstirred solution of HF (48%) at room temperature for four h to produce channels with an approximate depth of 365 μm. At the end of the etch period, the wafer was thoroughly rinsed with 18 MΩ water, the wax was removed, the photoresist was stripped and the thin films of Cr and Au were etched away.

3.8 *Characterization*

Quantitative channel-profile and surface roughness results were obtained using a Talysurf profilometer (Taylor-Hobson, UK) and an example is shown in Fig. 10. The average surface roughness of the etched microchannels (defined as the standard deviation of the bottom trace of the microcells) was 0.16 μm.

Qualitative results of the etched surfaces were obtained using optical- and video-microscopy. The surface of the walls was rough and, depending on the etchant, there was significant under-etching of the mask. SEMs are not shown due to lack of contrast.

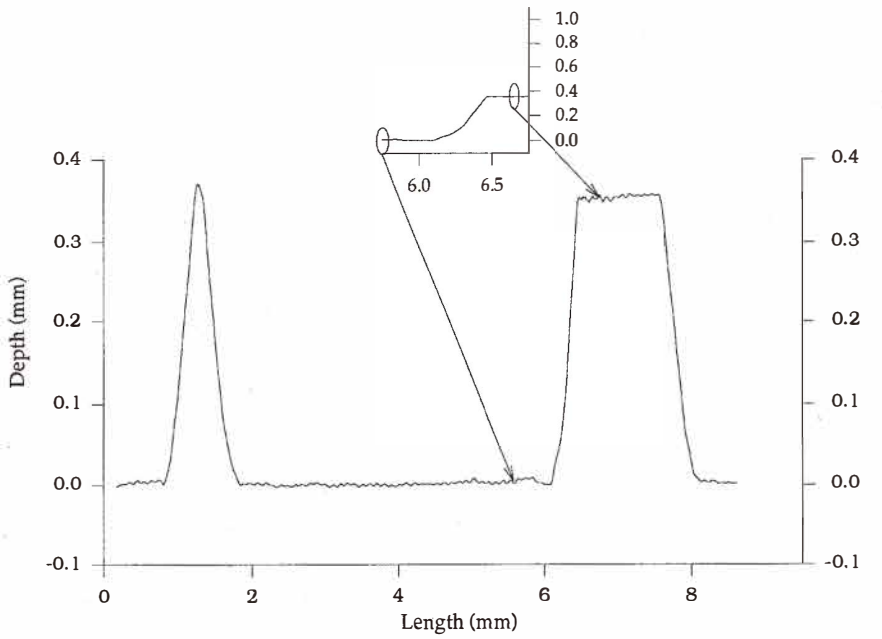

Fig. 10. Digitized profile of the microcell etched in quartz.

3.9 *Additional steps required for development of the microcell*

The wafer was diced to size at the Microtechnology Research Laboratory to produce three microcells. Two 1.6 mm holes were drilled at either end at the bottom of each microcell (Figs. 7(d) and 7(f)) to allow gas transport through the cell (once another quartz piece was clamped to the cell). Two thin-wall stainless steel tubes (3 cm in length and 1.6 mm in outer diameter) were affixed to the cell (Fig. 7(d)) using high temperature epoxy, and a rectangular piece of quartz was clamped onto the microcell, essentially forming an enclosed microcell akin to that shown in Fig. 7(a).

3.10 *Testing and potential future applications*

3.10.1 *Transmissivity*

Light transmission through the bottom of the etched microcells (Figs. 7(e) and 7(f)) was determined to be, on average, about 72%. This was determined by comparing the intensity of a Hg hollow cathode lamp (254-nm line) as measured using a PMT detector front-ended with a 0.35 m scanning monochromator (Heath Co.), with and without a microchannel in the radiation path.

3.10.2 *Atomic fluorescence of Hg*

The experimental set-up used to evaluate the microcell for *in-situ* measurement of atomic fluorescence of Hg-vapor-in-air is shown in Fig. 11. Due to poor etching quality, extensive masking of the front plate and of the edges of the cover-plate was required to reduce stray light arising from scattered radiation by the etched surfaces. This, in turn, increased background levels, reduced dynamic range and adversely affected detection limits.

The microcell was tested by injecting 100 μl of air saturated-in-Hg-vapor. Air samples were introduced into the injection port (Fig. 11) using a commercially available air-tight syringe. The home-made injection port that served as the sample introduction system had a dead volume of about 400 μl and the flow rate through the port was 60 ml per min. An example of the fluorescence signal obtained after a 100 μl injection is shown in Fig. 12 and the detection limit (3 σ) was 350 pg.

3.10.3 *Comparison*

For comparison, a commercially available 14.5 ml fluorescence-cell replaced the microcell in Fig. 11. Even with extensive optimization of operating conditions, fluorescence from Hg-vapor could not be obtained even after a 1000 μl injection of air-saturated-in-Hg-vapor. Clearly, a reduction in the volume of the measurement cell provided significant improvements in the sensitivity of Hg-vapor determinations. This is most likely due to favorable effects of scaling laws.

Due to the poor quality of current etched surfaces, the microcell is not attaining its full potential. Efforts are underway to reduce the amount of scattered light using, for example, anti-reflection optical coatings. Furthermore, the possibility of using plasma[10] or deep reactive ion etching[11] to anisotropically etch better quality, high aspect ratio microchannels in quartz rather than in Si is under investigation.

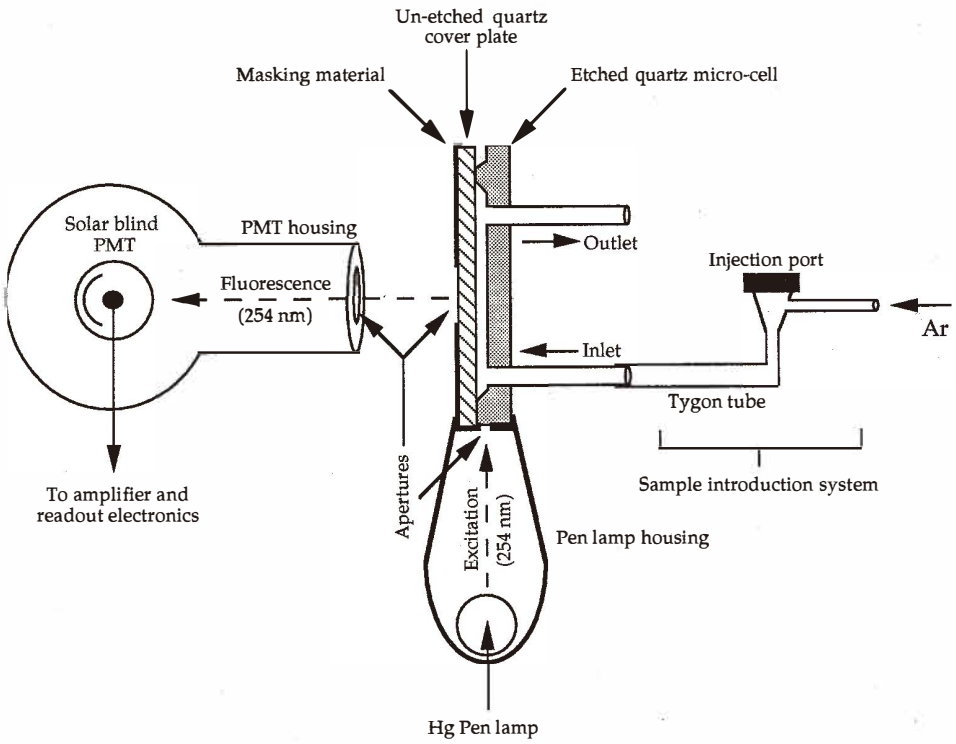

Fig. 11. Set-up for *in-situ* measurement of atomic fluorescence of Hg vapor.

4. Conclusions

The introduction of μl volumes of Hg-vapor into a μl UV-transparent measurement microcell resulted in considerable improvements in sensitivity and the use of spectroscopy in selectivity. Despite the poor quality of the etched surfaces, the UV-transparent microcell showed considerable promise for the determination of Hg-vapor-in-air by atomic fluorescence. In the future, such a cell may form the basis for the development of a portable/personal "sniffer" that can be used in the field for real-time environmental monitoring of Hg-vapor. The enclosed Si microchannel used as a sample introduction system for the measurement cell is expected to help miniaturize sample introduction, to reduce the dead volume of the current system and to further improve detection limits. Alternatively, replacement of the injector port (Fig. 11) by in-torch vaporization (ITV) sample introduction[12] is expected to open up new perspectives for the determination of Hg in liquid microsamples and thus expand the range and scope of applications of the UV-transparent measurement microcell.

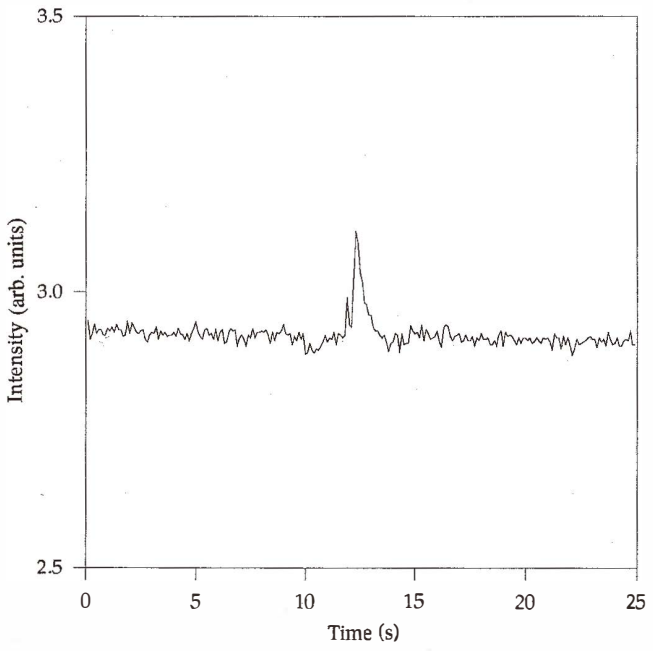

Fig. 12. Typical signal obtained by injecting 100 μl of air saturated in Hg-vapor.

Acknowledgments

Financial assistance from the University of Waterloo is gratefully acknowledged. Also, sincere thanks to Professor Arokia Nathan of the Department of Electrical and Computer Engineering of the University of Waterloo and to Professor Dr. Henry Baltes of the Institute of Quantum Electronics, Physical Electronics Laboratory, ETH, Zürich, Switzerland, for their invaluable contributions during the numerous discussions pertaining to miniaturization. Special thanks to personnel of the Microelectronics Research Laboratory (MRL) for their assistance.

References

1 V. Karanassios, J. T, Sharples and A. Nathan: Sensors and Materials, this issue.
2 N. R. Swart, M. Stevens, A. Nathan and V. Karanassios: Sensors and Materials, this issue.
3 Z. Zhang and V. Karanassios: Proceedings, Tech. Transf. Conf., Toronto, Ontario, 1993.
4 D. Choi: *"Neural Networks in ICP Spectrometry"*, Undergraduate Thesis, Department of Chemistry, University of Waterloo, 1996.
5 D. J. Harrison, K. Fluri, K. Seiler, Z. Fan, C. S. Effenhauser and A. Manz: Science **261** (1993) 895.

6 C. S. Effenhauser, A. Manz and H. M. Widmer: Anal. Chem. **65** (1993) 2637.
7 Z. H. Fan and D. J. Harrison: Anal. Chem. **66** (1994) 177.
8 S. C. Jacobson, L. B. Koutny, R. Hergenroder, A. W. Moore, Jr. and J. M. Ramsey: Anal. Chem. **66** (1994) 3472.
9 J. S. Daniel, F. Mitchel and G. Delapierre: Sensors and Actuators A **21–23** (1990) 971.
10 G. Dahm, I. W. Rangelow, P. Hudek and H. W. P. Koops: Microelectronic Engineering **27** (1995) 263.
11 Y. X. Li, P. J. French, P. M. Sarro and R. F. Wolfefenbuttel: Sensors and Actuators A **57** (1996) 223.
12 V. Karanassios, P. Drouin and G. G. Reynolds: Spectrochim. Acta **50B** (1995) 415.